Zitierweise: *Angew. Chem. Int. Ed.* **2024**, *63*, e202406924
doi.org/10.1002/anie.202406924

Pulsed CO_2 Electrolysis

Dynamics of the Boundary Layer in Pulsed CO_2 Electrolysis

*Matthias Heßelmann[+], Daniel Felder[+], Wenzel Plischka[+], Sajad Nabi, John Linkhorst[++], Matthias Wessling, and Robert Keller**

Abstract: Electrochemical reduction of CO_2 poses a vast potential to contribute to a defossilized industry. Despite tremendous developments within the field, mass transport limitations, carbonate salt formation, and electrode degradation mechanisms still hamper the process performance. One promising approach to tweak CO_2 electrolysis beyond today's limitations is pulsed electrolysis with potential cycling between an operating and a regeneration mode. Here, we rigorously model the boundary layer at a silver electrode in pulsed operation to get profound insights into the dynamic reorganization of the electrode microenvironment. In our simulation, pulsed electrolysis leads to a significant improvement of up to six times higher CO current density and 20 times higher cathodic energy efficiency when pulsing between −1.85 and −1.05 V vs SHE compared to constant potential operation. We found that elevated reactant availability in pulsed electrolysis originates from alternating replenishment of CO_2 by diffusion and not from pH-induced carbonate and bicarbonate conversion. Moreover, pulsed electrolysis substantially promotes carbonate removal from the electrode by up to 83% compared to constant potential operation, thus reducing the risk of salt formation. Therefore, this model lays the groundwork for an accurate simulation of the dynamic boundary layer modulation, which can provide insights into manifold electrochemical conversions.

[*] M. Heßelmann,[+] D. Felder,[+] W. Plischka,[+] S. Nabi, Prof. Dr.-Ing. J. Linkhorst,[++] Prof. Dr.-Ing. M. Wessling, Dr.-Ing. R. Keller
Chemical Process Engineering AVT.CVT
RWTH Aachen University
Forckenbeckstraße 51, 52074 Aachen, Germany
E-mail: robert.keller@avt.rwth-aachen.de

D. Felder,[+] Prof. Dr.-Ing. M. Wessling
DWI—Leibniz Institute for Interactive Materials e.V.
Forckenbeckstraße 50, 52074 Aachen, Germany

[+] These authors contributed equally.

[++] Current address: TU Darmstadt, Process Engineering of Electrochemical Systems, Otto-Berndt-Straße 2, 64287 Darmstadt, Germany

Introduction

Electrochemical reduction of CO_2 has become an industrially viable option in the development of carbon utilization technologies in recent years.[1] However, with systems for CO_2 conversion already reaching pilot scale and operating at industrially relevant production rates, research needs to focus on improving the process's energy efficiency, durability, and selectivity.[2] Pulsed electrolysis, i.e., the dynamic control of the cathode potential, has garnered increasing attention as an attractive tool to improve selectivity and durability of CO_2 electrolysis beyond steady-state operation.[3,4] Improvements in process selectivity and durability occur by adjusting the local reaction environment at the electrode, influenced by various effects.[6] The most relevant phenomena observed in pulsed electrochemical CO_2 reduction on silver electrodes, as studied in this work, can be summarized as weaker and stronger electrostatic attraction and repulsion, replenishment and depletion of CO_2, and salt removal and precipitation occurring at the reorganization and operation potential, respectively. Shiratsuchi et al.[7] reported stable and improved CO Faradaic efficiencies on a silver electrode in pulsed operation compared to potentiostatic operation. They concluded that rearrangement of the surface coverage with specifically adsorbed hydrogen atoms favors different reaction pathways. Thus, by regulating the magnitude of the cathodic potential pulse, Shiratsuchi et al. could tune the selectivity between methane and less hydrogenated molecules like CO and formic acid. Another influential parameter in pulsed electrolysis is the pulse duration step. Xu et al.[8] demonstrated almost two times higher current densities for CO_2 reduction when using pulse duration steps >0.5 s compared to chronoamperometric operation. The improved reaction rate in pulsed electrolysis is attributed to increased CO_2 accessibility resulting from recovery of the local reaction environment in the pulse off-time. Moreover, the long-term stability could be significantly improved over 25 hours of operation. The improvement in stable operation was more thoroughly investigated by the groups of Sargent and Sinton.[3] A detrimental phenomenon occurring in CO_2 electrolysis at high reaction rates is the precipitation of carbonate salts due to increased local alkalinity. This leads to flooding and blockage of reactant transport paths in the gas diffusion electrode. However, pulsing the applied potential between the operating potential and a lower regeneration potential forces carbonate ions to migrate away from the cathode during

the regeneration period. Hence, the carbonate concentration in the immediate cathode catalyst environment could be significantly reduced, and stable operation of more than 236 h was achieved. In recent work, Lu et al.[9] used optical coherence tomography to visualize the dynamics of reactions and mass transport of gas and liquid phases within a silver gas diffusion electrode during galvanostatic and pulsed operation. They showed that applying a square-wave current profile helps to substantially remove accumulated gas bubbles in the porous electrode, which significantly reduces the electrochemically active surface area within the electrode and, thus, productivity. Besides the aforementioned improvements in controlling reaction pathways, modulating mass transport, and regulating the local pH discussed for silver electrodes, the literature on pulsed electrolysis also reports changes to the catalyst, e.g., electrode restructuring and surface roughening of copper catalysts, enhancing the electrochemical performance.[10,11] However, these effects are beyond the scope of this work. The local reaction and mass transport phenomena are difficult to resolve in the respective length and time scales using experimental techniques, thus calling for mathematical approaches to reveal the complex species-electrode interactions. Bui et al.[12] developed a transient continuum model of the boundary layer (BL) in COMSOL Multiphysics to study local pH effects and reactant transport by applying various pulse shapes. They found that the enhancement in selective CO_2 reduction to multicarbons not only results from high CO_2 concentrations but also from high pH values and overpotentials. However, the model neglects steric effects of ions, which become relevant in the considered potential regimes and significantly influence the local reaction conditions at the electrode.[13–15] Moreover, the electroneutrality assumption in their model does not hold for the immediate electrode region.[16] Bohra et al.[14] and later Butt et al.[15] demonstrated that a size-modified expression of the Poisson-Nernst-Planck equation is necessary to adequately model the local mass transport in the immediate electrode environment. Several researchers have implemented the generalized modified Poisson-Nernst-Planck or the size-modified Poisson-Nernst-Planck to obtain a more realistic and complete representation of the electric double layer (EDL) in CO_2 electrolysis.[14,15,17–20] While these models cover asymmetric electrolytes with multiple ion species and finite ion sizes over a wide range of potentials and length scales, the system of equations is numerically challenging and computationally demanding, thus, electrochemical reactions are mostly simplified, and only steady-state solutions are presented.[13,21] However, to elucidate the underlying mass transport and reaction phenomena in pulsed CO_2 electrolysis, rigorous consideration as transient modeling, are indispensable. Here, we present a time-dependent continuum model of the BL at a silver planar plate electrode using the size-modified Poisson-Nernst-Planck model to describe mass transport and the Frumkin-corrected Tafel kinetic expression to

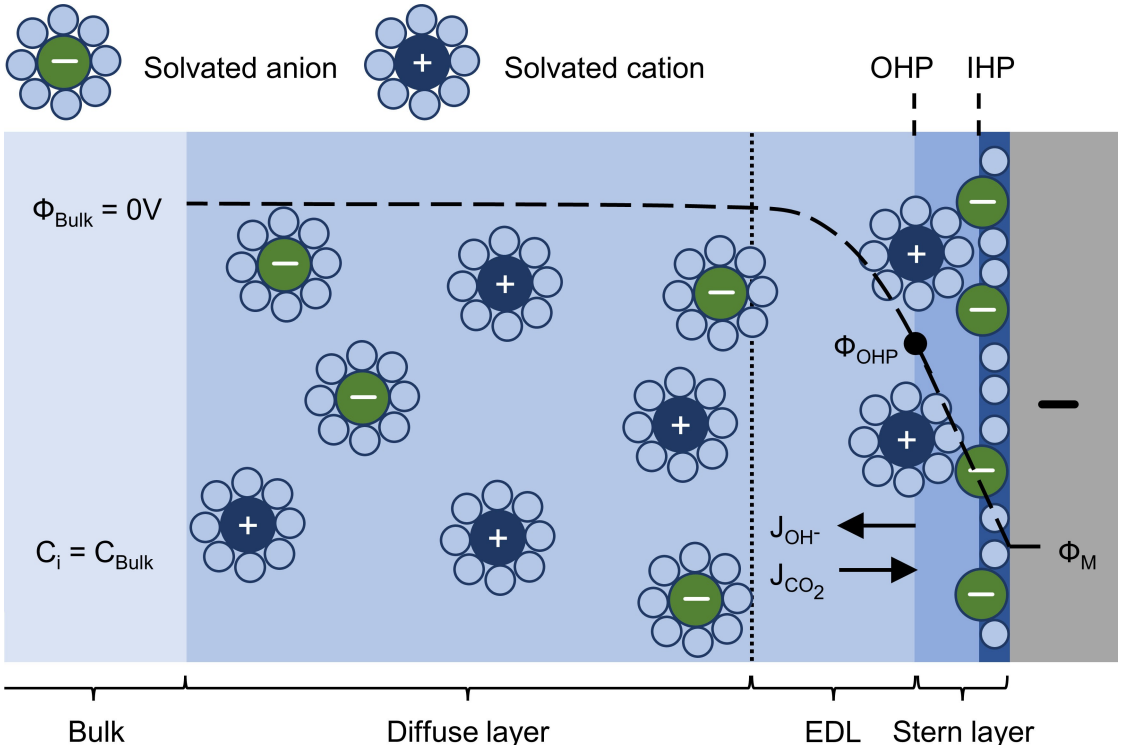

Figure 1. Schematic illustration of the BL modeled in COMSOL Multiphysics 6.1. IHP and OHP stand for the inner and outer Helmholtz plane, respectively. In the following, the domain where electroneutrality is not maintained is referred to as EDL. The illustration was adapted from Bard et al.[5]

account for the electrochemical reactions. The model is used to study the electrochemical CO_2 reduction in constant potential and pulsed operation to elaborate the mechanisms leading to the differences in reaction rate and selectivity between the two modes. Moreover, we investigate the influences of pulse duration and potential amplitude to derive guidelines for optimizing pulsed electrolysis.

Results and Discussion

Figure 1 sketches the BL at a silver planar plate cathode simulated in this work. A one-dimensional model was implemented as the concentration and potential gradients orthogonal to the electrode surface are of particular interest. The domain of the model is confined by the two boundaries, i.e., the outer Helmholtz plane and the bulk solution. The model equations were implemented and solved in COMSOL Multiphysics 6.1. More details are described in the SI.

In the results section, we first discuss the model validity and elaborate on mass transport limitations typically observed at constant potential operation. Afterward, we present and discuss the comparison to pulsed electrolysis when applying different pulse profiles. The kinetic parameters in Equation (S14)–(S15) were determined by fitting the model to experiments from Hatsukade et al.[22] carried out in an electrochemical flow cell with an aqueous 0.1 M $KHCO_3$ electrolyte solution and silver foil as the cathode. For the parameter estimation, a BL thickness of 150 µm was assumed based on a similar value reported by Weng et al.[23], who also used the data of Hatsukade et al. for validation. A more detailed description of the kinetic parameter estimation is described in the SI. The polarization curve in Figure 2(a) shows a good fit of the simulated total current densities with the experimental values. Furthermore, the limiting current density for the electrochemical CO_2 reduction in the simulation is in good agreement with the experimental study, as shown in Figure 2(b). However, the model slightly overestimates the CO current density in the low and high potential regimes. Also, the simulated partial current density for the HER in Figure 2(c) is higher than the measured partial current densities between potentials of −1.35 V vs SHE and −1.75 V vs SHE. Besides the uncertainty in the model parameters taken from the literature, the potential of zero charge, the boundary layer thickness, and the charge transfer reaction kinetics are not explicitly known for the experimental system of Hatsukade et al. For a more accurate fit, the potential of zero charge and the boundary layer thickness must be determined experimentally. Nevertheless, the fitted parameters are in a reasonable range,[24] and the model matches the order of magnitude of the experimental results and shows good agreement with the trends observed in the study by Hatsukade et al. To show the dependency of the simulation results on the assumed BL thickness, simulations with BL thicknesses of 100 µm and 50 µm are presented in Figure S1–S2. As expected, the attainable CO current densities shift to higher values due to shorter distances for mass transport from the bulk phase to the reaction plane. Also, the limiting current density increases and deviates from the value measured in the work of Hatsukade et al.

In the constant potential simulations carried out for the model validation, the CO_2 concentration in the BL significantly drops when increasing the potential from −1.05 V vs SHE to −1.85 V vs SHE, as indicated in Figure 3(a). At −1.85 V vs SHE, CO_2 is almost completely depleted in the BL, resulting in the observed decrease in the CO_2 reduction rate in Figure 2(b). Figure S3(b) presents the temporal evolution of the CO_2 concentration in the BL at −1.85 V vs SHE. The CO_2 concentration in the BL drops almost to zero after only a few hundred milliseconds and reaches a steady state at around 10 s, as shown by the CO current density over time in Figure S3-(a). The sudden increase in CO current density at around 2.0 E-07 s is due to the initial charging of the EDL. The initial peak due to the charging current is much larger than the faradaic current for the reduction reaction and

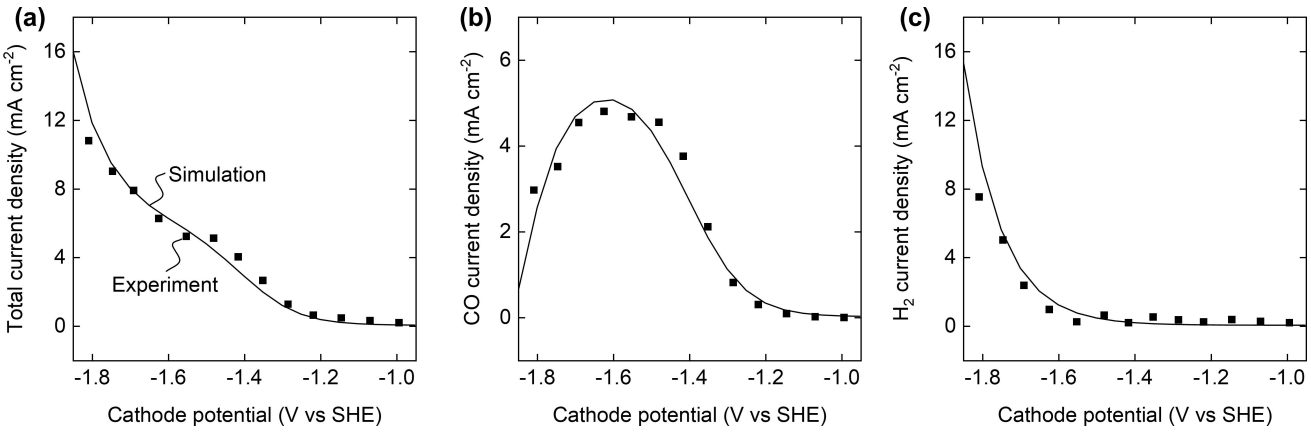

Figure 2. Experimental (points) and simulated (curves) total (a) and partial current densities for the electrochemical CO_2 reduction to CO (b) and the HER (c) as a function of the applied cathode potential. The experimental data was taken from Hatsukade et al.[22]

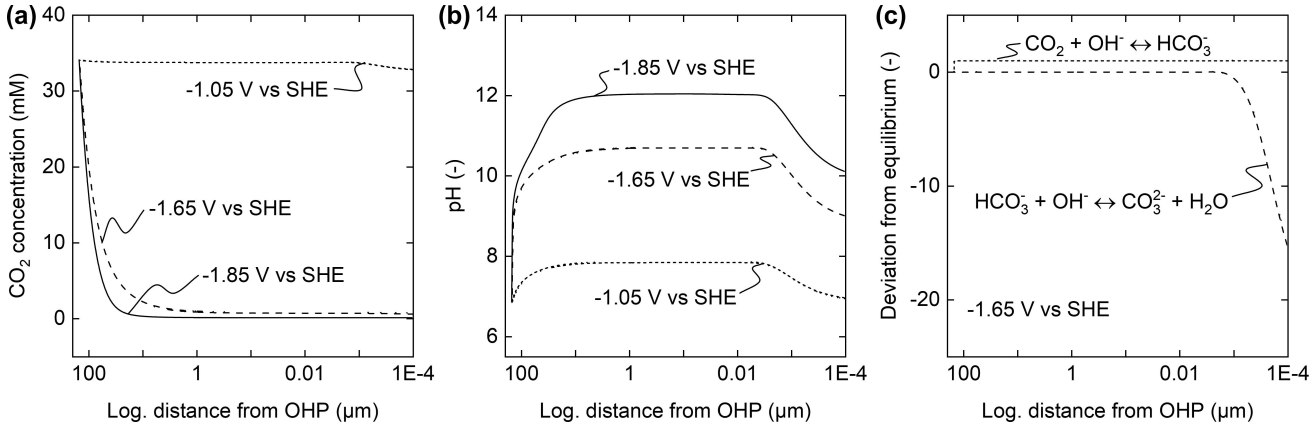

Figure 3. CO_2 concentration (a) and pH (b) in the BL (150 μm) in steady-state over the logarithmic distance to the OHP, and the deviation from the equilibrium of reactions (S8)-(S9) in the BL at a potential of −1.65 V vs SHE (c). A deviation of 1 corresponds to a much faster forward than backward reaction rate. The dissociation reactions are in equilibrium if the deviation is 0. At highly negative values, the backward reaction rate is much faster than the forward reaction rate.

can usually not be resolved experimentally as the EDL charging is completed after a few ms.[5,25,26] Only when decreasing the data acquisition time of potentiostatic measurements as low as 0.2 ms Bui et al.[12] could show the EDL charging experimentally. For an applied potential of −1.05 V vs SHE, the CO_2 concentration only changes slightly along the BL as the diffusion of CO_2 is faster than its consumption rate in the electrochemical reduction reaction. Only in the first 1 nm of the EDL does the CO_2 concentration slightly drop to 32.6 mM. Simultaneously, Figure 3(b) shows an increase in the pH in the BL from 6.8 in the bulk electrolyte to 7.8 and 12.0 for −1.05 V vs SHE and −1.85 V vs SHE, respectively. The trends observed for the pH in the BL are also in good agreement with CO_2 electrolysis experiments on Ag foam in a flow cell conducted by Zhang et al.[27] using operando Raman spectroscopy. In the simulations of this work, the pH at the immediate electrode surface drops to 6.9 at −1.05 V vs SHE and 9.9 at −1.85 V vs SHE. The strong pH decrease close to the OHP is due to the electrostatic repulsion of OH– ions and the attraction of H^+ at the negatively charged electrode and cannot be resolved with the techniques used by Zhang et al.

The significant changes in the local pH affect the dissociation reactions (S8)–(S10) as indicated by the plotted deviation from the equilibrium in Figure 3(c). The calculation of the deviation from the dissociation equilibrium is calculated as presented in Equation (S25). The dissociation reaction between HCO_3^- and CO_3^{2-} is in equilibrium for almost the entire domain. Only in the range from 2 nm to the OHP, the dissociation equilibrium is strongly shifted to the bicarbonate side of Reaction (S8). The negative deviation from the equilibrium of Reaction (S8) is most likely attributed to a combination of the dropping pH value and the electrostatic repulsion of HCO_3^- at the electrode surface. The deviation of the dissociation reaction of CO_2 to HCO_3^- (Reaction (S9)) is 1 for the entire domain indicating that CO_2 is steadily consumed in the BL because of the high alkalinity in the near-electrode region and sluggish reaction kinetics of the backward reaction.[28] Thus, HCO_3^- does not act as a resupply for CO_2 at the electrode vicinity. Moreover, the consumption of CO_2 in the dissociation reactions results in increased CO_3^{2-} formation at elevated potentials, as shown in Figure S4(c). Similar findings were also recently shown experimentally by Jovanovic et al.[29] using in operando NMR spectroscopy. However, the dissociation rates could be shifted by tuning the electrolyte cations' catalytic properties.[30]

The presented results highlight the importance of modulating the local electrode environment, i.e., reactant concentration and pH value, to improve reaction activity and selectivity. Herein, we discuss the effects of applying various pulsed potential profiles on the activity and selectivity of electrochemical CO_2 reduction by improving mass transport and local reaction conditions. The simulated pulse profile with an operation potential of −1.65 V vs SHE and a regeneration potential of −1.05 V vs SHE is depicted in Figure 4(a). Each potential was held for 1.0 s.

When applying the first pulse, the potential at the OHP in Figure 4(b) responds with a jump from −0.77 V vs SHE to −0.96 V vs SHE and a subsequent decrease to −0.90 V vs SHE, after which the cathode potential is switched to the regeneration potential. The initial peak results from the enhanced charging of the EDL when increasing the electrode potential and occurs repeatedly when switching to the operation potential. However, the peak height decreases with the number of "on-pulses" (pulses at operation potential) and stays constant after four pulses. Similar behavior of the trend in peak intensity is also seen for the CO current density in Figure 4(c) and was also observed experimentally by Bui et al.[12] Even though Figure S6 shows a significant charge build-up in the immediate electrode environment at the first on-pulse, charge conservation in the EDL cannot be the main reason for the trend in the peak heights as the free charge density before the seventh pulse is only slightly higher than before the first pulse. Moreover, the charge passed

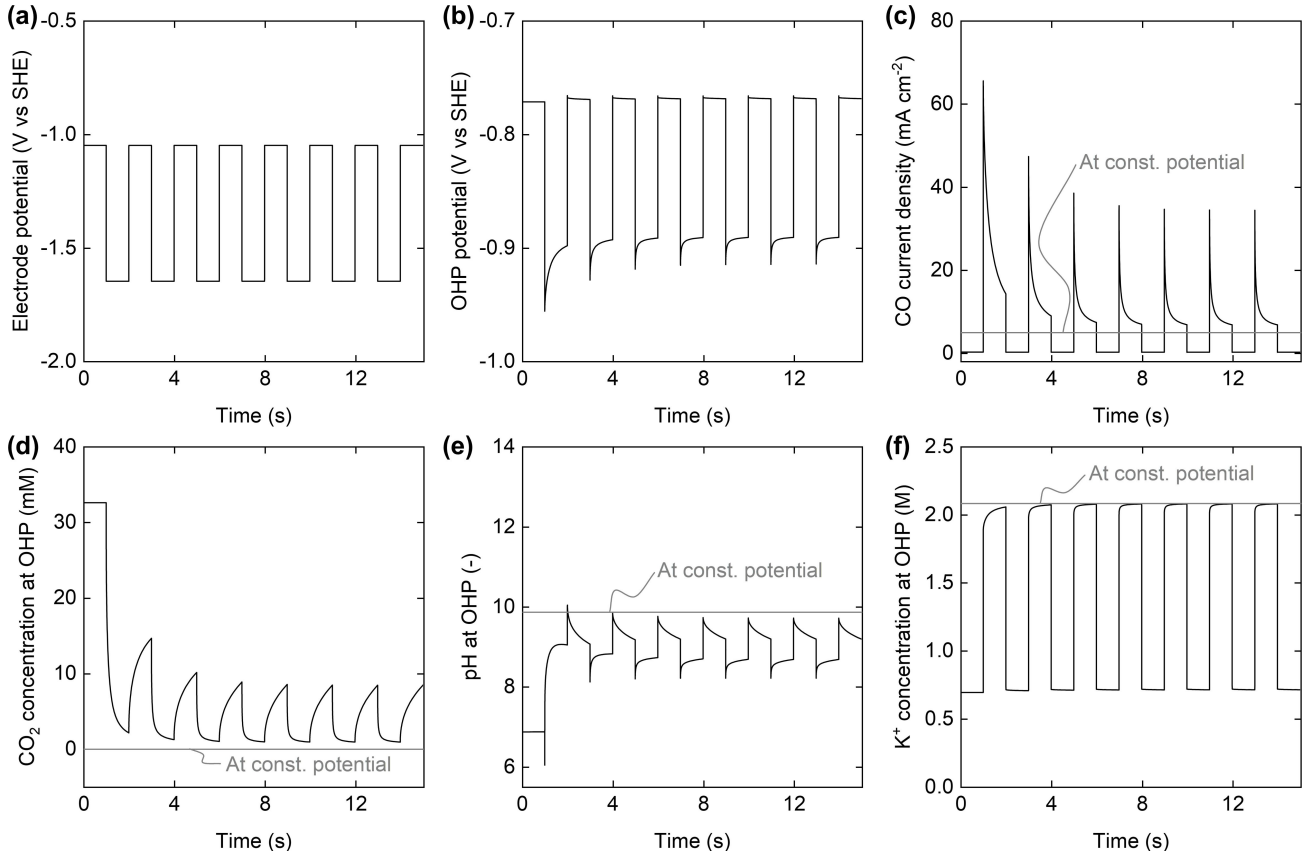

Figure 4. Applied cathode potential (a), the potential at the OHP (b), CO current density (c), and the CO_2 concentration (d), pH (e), and K^+ concentration (f) at the OHP when applying a pulse profile with an operation potential of −1.65 V vs SHE and regeneration potential of −1.05 V vs SHE with a pulse duration of 1.0 s. The pulsed operation is started after a 15 s initialization phase at −1.05 V vs SHE. The grey lines refer to the results of the constant potential operation.

during each "off-pulse" (pulse at regeneration potential) remains fairly constant. Therefore, rather the adjusting CO_2 concentration at the OHP in Figure 4(d) due to alternating depletion and regeneration, i.e., diffusive transport to the electrode, limits the attainable current than the built-up of charge in the EDL.

At the beginning of each off-pulse, the OHP potential reveals a small peak attributed to charge release when switching from the high operation to the low regeneration potential. The current density signal attributed to charge release is only visible when using a logarithmic scale, as shown in Figure S5 The elevated CO current density in Figure 4(c) during the on-pulse compared to the CO current density at constant potential operation (grey line) is mainly because of the higher CO_2 availability at the electrode surface, as indicated by the CO_2 concentration at the OHP in Figure 4(d). These results highlight the beneficial effect on reactant availability in pulsed electrolysis compared to constant potential operation. Interestingly, the CO_2 concentration strongly increases right at the beginning of each off-pulse, attributed to a large concentration gradient between the bulk electrolyte and the OHP, but then starts stagnating as the diffusive driving force diminishes. Hence, long regeneration times might be less efficient in terms of reactant replenishment than short ones. The influence of the pulse duration will, therefore, be discussed later on.

The H^+ concentration at the OHP, depicted by the pH value in Figure 4(e), shortly increases when applying the operation potential at 1.0 s and then decreases until a steady value is reached. The respective pOH is shown in Figure S9. The current density rises, OH^- is produced in the charge transfer reactions, and thus, the pH increases until it is balanced with surface H^+ ions. When switching to the regeneration potential at 2.0 s, the pH first increases as the attraction of H^+ decreases, and a high amount of OH^- ions is still present at the OHP before hydroxide diffuses into the diffuse layer, resulting in the decreases in pH. In the following pulses, the pH level is slightly lower than in the first one due to the lower production of OH^-, indicated by the CO current Figure 4-(c). As a result of the lower pH in pulsed electrolysis compared to constant potential operation, the concentration level of CO_3^{2-} in short decrease in pH at the beginning of the pulse can be explained by the electrostatic attraction of protons due to the potential increase. However, as Figure S7(a)–(b) is also reduced. Accordingly, Figure S8 shows that the amount of HCO_3^- averaged over the BL thickness increases in pulsed electrolysis.

The K^+ ions in Figure 4(f) almost instantly build up when switching to the operation potential due to the high mobility of K^+. Therefore, it is expected that the beneficial co-catalytic properties of K^+ in electrochemical CO_2 reduction are not impaired during the on-pulse. While the trend of the cation concentration observed here is comparable to other works on simulating pulsed electrolysis, the absolute concentrations at the OHP are significantly higher.[12] The electroneutrality assumption in the work of Bui et al.[12] gives a good estimate of concentrations and the electric field in most parts of the BL. However, this assumption fails in the EDL, i.e., the local reaction environment in the immediate electrode region.[18,31] Thus, charge-dependent electric field phenomena and the consideration of steric effects are indispensable when simulating the dynamic reorganization at the electrode surface.

For a more thorough analysis of the effect of pulse settings on CO_2 electrolysis performance indicators, i.e., CO current density, faradaic efficiency, and cathodic energy efficiency, the pulse duration and the operation potential were varied in Figure 5. Time-averaged values were calculated for pulsed operation by integrating over the last on- and off-pulse at each setting to compare the results from pulsed electrolysis with constant potential operation. The average CO current density in Figure 5(a) at potentials of −1.45 V vs SHE and −1.65 V vs SHE is lower than the steady-state CO current density in constant potential operation for all studied pulse durations even though the average CO_2 concentration at the OHP is higher, as shown in Figure 5(d). Among the simulated potentials, pulsed operation only leads to a significant improvement in the CO production rate from 0.6 mA cm^{-2} in constant potential operation to 3 mA cm^{-2} in pulsed operation at −1.85 V vs SHE and a pulse duration of 0.5 s. At this point, the average CO current density at −1.85 V vs SHE even exceeds the one at −1.45 V vs SHE. For one, the average CO current density trend is driven by the available CO_2 at the OHP. In the mass-transport-limited potential regime, i.e., at −1.85 V vs SHE, the alternating replenishment of CO_2 at the reaction plane helps to overcome the imbalance between reactant consumption and its diffusive transport to the electrode. However, even though a regeneration time of more than 3.7 s is required for a CO_2 molecule to diffuse through the BL, as approximated using Equation (S31), Figure 6(d) shows that partial replenishment of CO_2 at the OHP at shorter pulses is sufficient to increase the CO current

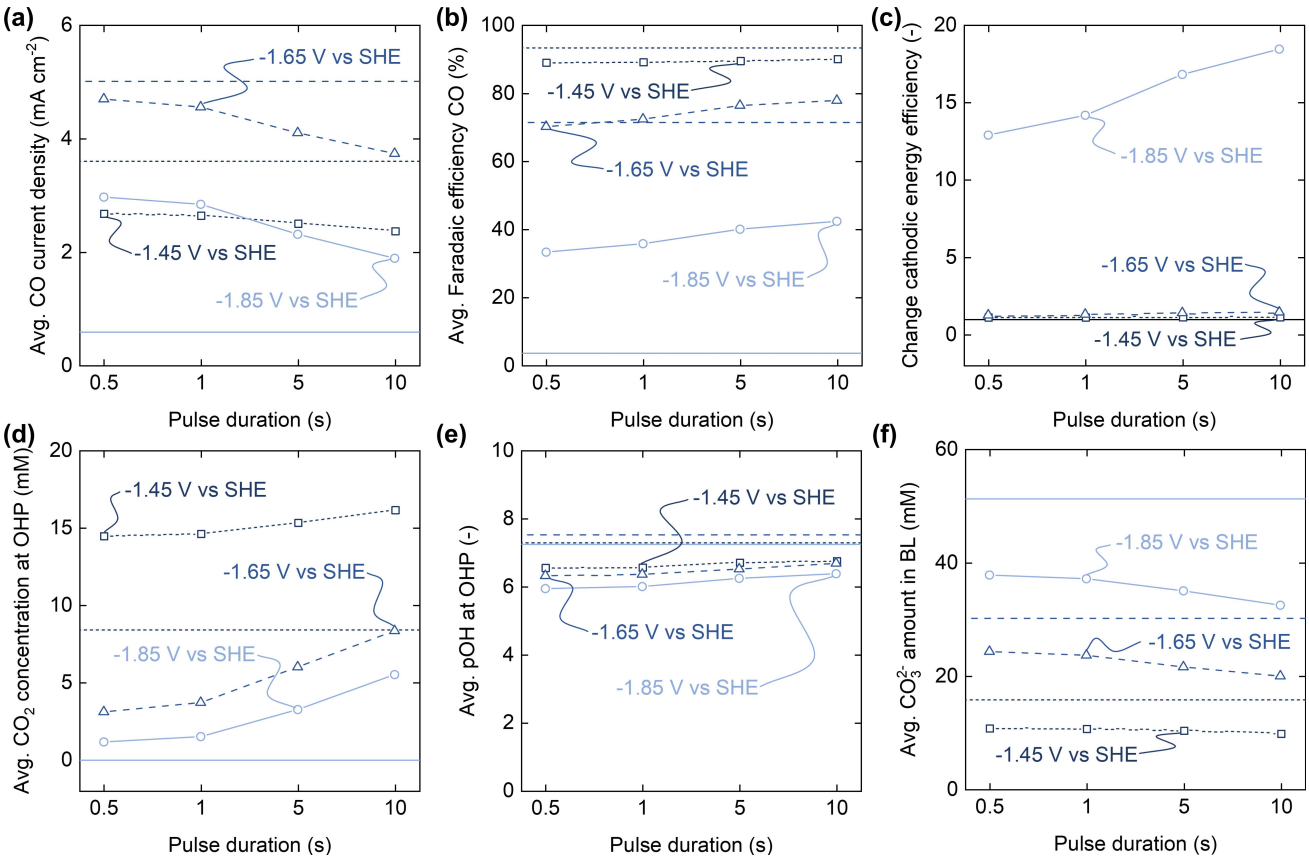

Figure 5. Average values of the CO current density (a), the Faradaic efficiency for CO (b), the change in cathodic energy efficiency compared to constant potential operation (c), the CO_2 concentration (d) and pOH (e) at the OHP and the amount of CO_3^{2-} in the BL (f) when applying pulse profiles with an operation potential of −1.45 V vs SHE, −1.65 V vs SHE, and −1.85 V vs SHE and regeneration potential of −1.05 V vs SHE with various pulse duration (on- and off-pulse). The pulsed operation is started after a 15 s initialization phase at −1.05 V vs SHE. The lines without symbols refer to the results of the constant potential operation at the respective applied operation potentials. The x-axis is not linear, and lines between symbols should only help the reader's eye.

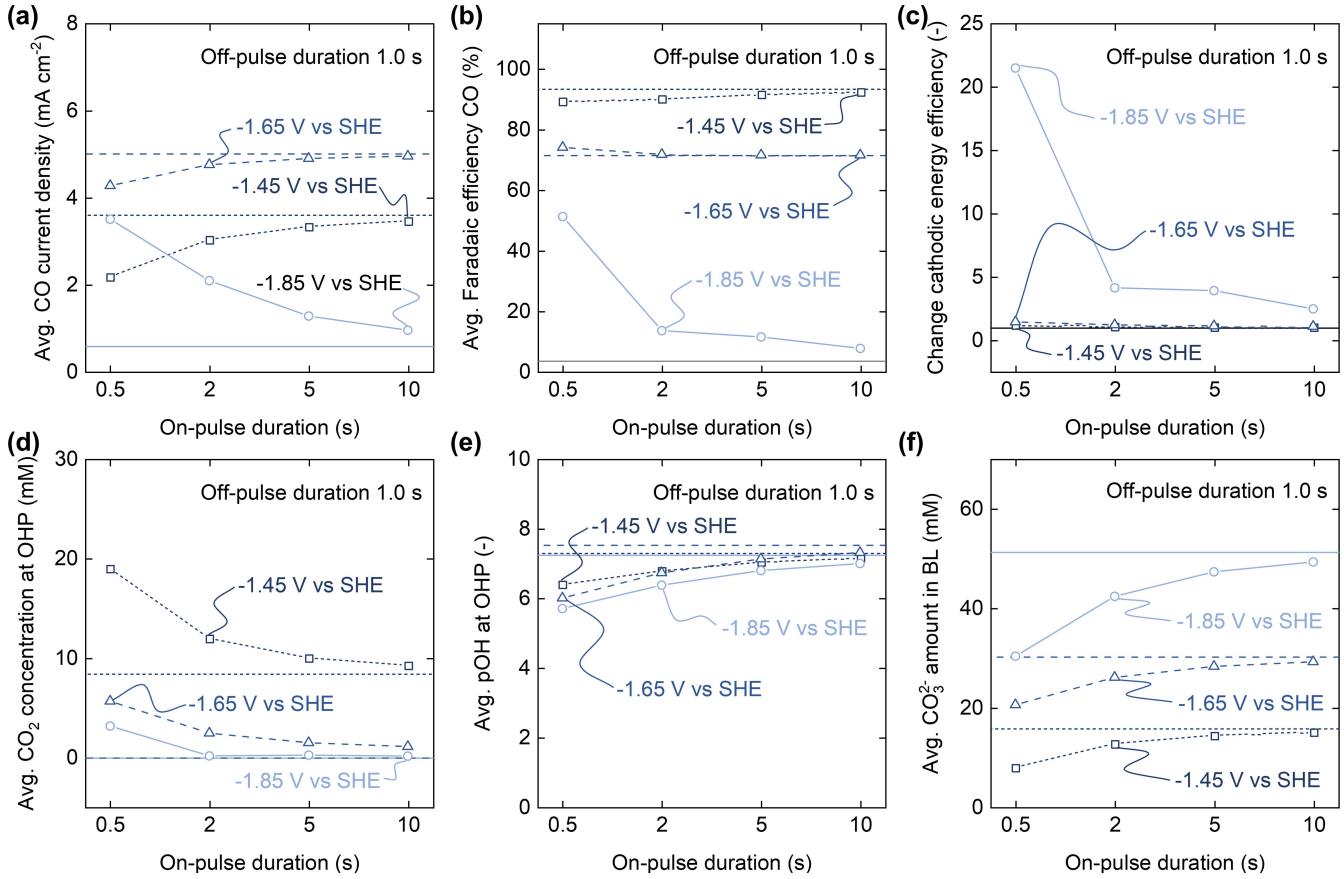

Figure 6. Average values of the CO current density (a), the Faradaic efficiency for CO (b), the change in cathodic energy efficiency compared to constant potential operation (c), the CO_2 concentration (d) and pOH (e) at the OHP and the amount of CO_3^{2-} in the BL (f) when applying an asymmetric pulse profile with an operation potential of −1.45 V vs SHE, −1.65 V vs SHE, and −1.85 V vs SHE and regeneration potential of −1.05 V vs SHE with an off-pulse duration of 1.0 s. The pulsed operation is started after a 15 s initialization phase at −1.05 V vs SHE. The grey lines refer to the results of the constant potential operation at the respective applied operation potentials. In graph (c), the grey line at 1 indicates that the cathodic energy efficiency does not change in pulsed operation compared to constant potential operation. The x-axis is not linear, and lines between symbols should only help the reader's eye.

density. Hence, short pulses are more effective in allowing partial regeneration of the BL while avoiding a state of reactant limitation. In the case of BL thicknesses < 150 µm, as shown in Figure S1–S2, even shorter pulse times might be needed in pulsed electrolysis to outperform constant potential operation. The general trend of decaying CO current density with pulse duration was also shown experimentally by Arndt et al.[32] in an H- cell with a silver foil as the cathode. At −1.45 V vs SHE and −1.65 V vs SHE, however, the CO_2 availability is not yet limiting, and the mass transport and consumption at the electrode are in equilibrium, respectively. Thus, the lower CO current density at −1.05 V vs SHE during the off-pulse compromises the average CO current density. The impact of the off-pulse decreases at shorter pulses, and the average CO current density gets closer to constant potential operation. To compensate for the low production rate during the off-pulse, a regeneration potential of −1.45 V vs SHE was simulated in Figure S10. In this case, the average CO current density at an operating potential of −1.65 V vs SHE and a pulse duration of 1.0 s can only be slightly improved from 4.7 mA cm^{-2} to 4.8 mA cm^{-2}. While the time-averaged CO current density during the off-pulse is increased from 0.01 mA cm^{-2} at a regeneration potential of −1.05 V vs SHE to 1.8 mA cm^{-2}, the CO current density during the on-pulse decreases from 9.1 mA cm^{-2} to 7.7 mA cm^{-2} due to the lower CO_2 concentration at the OHP (2.5 mM) when regenerating at a higher cathodic potential, as shown in Figure S10(b). Hence, the combined performance during on- and off-pulse would benefit from an elevated regeneration potential, but sufficient replenishment of CO_2 must be ensured.

Whereas short pulses lead to a higher average CO production rate than longer pulses, the CO Faradaic efficiency in Figure 5(b) increases with the pulse duration. A similar trend is also observed for the change in cathodic energy efficiency related to the constant potential operation, as shown in Figure 5(c). The cathodic energy efficiency is defined by the energy consumed in the reduction of CO_2 related to the applied energy at the cathode, according to Equation (S26). Again, pulsed electrolysis significantly improves Faradaic efficiency at −1.85 V vs SHE by a factor of 11 at an on-pulse duration of 10 s compared to constant

potential operation and also leads to an 18 times higher cathodic energy efficiency at the same settings. The enhancement is reflected in the average values of the complete on- and off- pulse and the average values of only the on-pulse. The CO Faradaic efficiency averaged over the time of the on-pulse only at, e.g., a pulse duration of 10 s and −1.85 V vs SHE is 15.7 %, as shown in Figure S11. This increase compared to constant potential operation is attributed to the sufficient replenishment of CO_2 at the OHP with long pulses and thus enough time to allow CO_2 to diffuse from the bulk to the electrode, as shown in Figure 5-(d). At a pulse duration of 10 s and −1.65 V vs SHE, the average on-pulse CO Faradaic efficiency is 76.4 %, which is close to the value in constant potential operation. The improvement in the average value in Figure 5(b) is therefore also attributed to the higher CO Faradaic efficiency at the regeneration potential, which is 79.2 % on average during the off-pulse. These findings show promising improvement in pulsed electrolysis compared to constant potential operation at the same operating potential. However, when comparing different potentials, e.g., between pulsed operation at −1.85 V vs SHE and constant potential operation at −1.65 V vs SHE, at which the highest CO production rate is achieved, the cathodic energy efficiency is approx. 2.0 times lower at a pulse duration of 0.5 s and 1.6 times lower at 10.0 s.

Apart from the improvements in CO_2 mass transport due to alternating regeneration of the near-electrode region, Sinton and co-workers[3] suggested pulsed electrolysis as a self-cleaning approach to prevent carbonate salt formation in membrane electrode assemblies and thus improve long-term operation stability. Figure 5(f) shows that the level of the CO_3^{2-} amount in the BL is lowered in pulsed operation compared to constant potential operation. The reduction in CO_3^{2-} in pulsed electrolysis is mainly attributed to enhanced diffusive removal during the off-pulse. As the deviation from the equilibrium in Reaction (S8) at the OHP in Figure S12(a) is small, the dissociation rate of CO_3^{2-} to HCO_3^- is low. Thus, the decreasing CO_3^{2-} can only be explained by diffusive transport from the BL into the bulk solution. Attributed to enhanced regeneration of the BL at long pulse durations (5 s and 10 s), the amount of CO_3^{2-} decreases even further. Applying a pulse duration of, e.g., 10 s leads to a 37 % reduction of CO_3^{2-} in the BL at 1.85 V vs SHE compared to constant potential operation. In the work of Sinton et al., much longer off-pulse durations of 30 s were used, which could explain the enhanced self-cleaning effect even at higher current densities that were obtained due to the use of porous catalyst layers. Also, Cofell et al.[33] showed a 51 % reduction in surface CO_3^{2-} deposits at similar conditions using an Ag gas diffusion electrode in an electrochemical flow cell. Hence, pulsed electrolysis can be used as a strategy to circumvent carbonate accumulation near the electrode and, therefore, mitigate the risk of salt precipitation, especially in gas diffusion electrodes. Interestingly, the amount of HCO_3^- in the BL increases in pulsed operation compared to constant potential operation, as shown in Figure S13. Whereas high alkalinity in the BL attributes a high ratio of CO_3^{2-} to HCO_3^- at elevated potentials, HCO_3^- diffusion into the BL during the off-pulse leads to an overall increase in HCO_3^- the whole pulse period.

It needs to be mentioned that our model is limited to mass transport and kinetic phenomena in the BL and does not resolve ion and reactant adsorption and desorption on the electrode surface. However, cations and anions also interact with the electrode through, e.g., specific adsorption, which has been shown to stabilize or destabilize reaction intermediates.[34,35] To get a more comprehensive picture of how the reorganization of the BL induced by pulsed electrolysis affects the adsorption and desorption of ions and reaction intermediates on the electrode and, thus, the charge transfer reactions, future modeling work should consider microkinetic reaction models.[36] Moreover, pulsed electrolysis leads to morphological changes of the catalyst surface, affecting the charge transfer reactions as thoroughly investigated for copper catalysts.[37–40] However, the number of publications on surface structural changes of silver electrodes in pulsed operation is small, and thus, there is no comprehensive understanding of these effects on electrolysis performance yet.[41]

To further tweak the electrolysis performance by modulating the pulse settings, asymmetric pulses with constant off-pulse duration and changing on-pulse duration were studied in Figure 6. While the CO current density with symmetric pulses in the non-transport-limited potential regime is beyond what is obtained in constant potential operation, similar values are reached for −1.45 V vs SHE and −1.65 V vs SHE with asymmetric pulses at an on-pulse duration of 10.0 s. The larger the ratio of on-pulse duration to off-pulse duration gets, the closer the pulsed operation mode approaches constant potential operation, and thus, the time-averaged performance indicators approach similar values. In contrast to the plateauing trend in the average CO current density with symmetric pulses at short pulse durations, Figure 6(a) shows a progressive improvement in CO production rate with shorter on-pules at −1.85 V vs SHE but a decaying trend for −1.45 V vs SHE and −1.65 V vs SHE. At potentials in the mass-transport-limited regime above −1.65 V vs SHE, CO_2 in the BL is rapidly depleted, as shown in Figure S3. Consequently, short on-pulse durations are more desirable to reduce the influence of CO_2 diffusion limitation. However, at −1.45 V vs SHE and −1.65 V vs SHE, the Faradaic CO current at the beginning of the on-pulse is not large enough to balance the low CO current density during the off-pulse. Therefore, the average CO current density approaches the value at the regeneration potential at shorter on-pulses. A similar trend is also expected at −1.85 V vs SHE for even shorter on-pulses than 0.5 s. The increased CO_2 concentration at the OHP at short on- pulses again results in a significant improvement in the CO Faradaic efficiency and cathodic energy efficiency at −1.85 V vs SHE and even exceeds the best performing symmetric pulse settings, as shown in Figure 6(b)–(c). Surprisingly, whereas the efficiency of pulsed electrolysis is beyond constant potential operation in simulations in Figure 5, in asymmetric pulse operation with an on-pulse duration of 0.5 s at −1.85 V vs SHE, the energy efficiency is the same as in constant potential operation at −1.65 V vs

SHE, as concluded from Table S2. Additional simulations with an on-pulse duration of 0.3 s at −1.85 V vs SHE in Figure S15(a) showed that the time-averaged CO current density could be slightly increased to 3.6 mA cm^{-2} without compromising cathodic energy efficiency. The improvements due to asymmetric pulses highlight the need for more sophisticated approaches to find suitable pulse settings to exploit the full potential of pulsed CO_2 electrolysis. Frey et al.[42] applied Bayesian optimization for pulsed operation to optimize an intentionally unoptimized experimental setup and achieved a CO current density increase by >64 % compared to the initial system. Besides optimizing the pulse settings, i.e., the applied potentials and the pulse duration of the on- and off-pulse, other experimental design parameters, such as the electrolyte flow rate, the electrolyte concentration, and various electrode geometries, need to be considered when optimizing pulsed CO_2 electrolysis in terms of current density and energy efficiency. Especially porous gas diffusion electrodes will be of particular interest for mathematical simulation and optimization in pulsed operation due to their significant industrial relevance for electrolysis processes and the more complex interplay of mass transport and reaction phenomena to be modulated. Nevertheless, the model presented here lays the groundwork for combining simulation and optimization of pulsed CO_2 electrolysis in a less costly and time-consuming manner and, therefore, also rapid design of experiments. At −1.45 V vs SHE and −1.65 V vs SHE, the CO Faradaic efficiency behaves similarly to the CO current density and approaches the Faradaic efficiency at the operation and regeneration potential at long and short on-pulses, respectively. Surprisingly, even though the electrode produces more OH^- at −1.85 V vs SHE and short on-pulses compared to constant potential operation and long on-pulses as deduced from the elevated CO current density in Figure 6(a), the CO_3^{2-} amount in the BL decreases for shorter on-pulses. It is also noteworthy that the time-averaged amount of CO_3^{2-} in the BL at an on-pulse duration of 0.3 s in Figure S15(b) can be decreased to 26 mM, which is even below the CO_3^{2-} amount at constant potential operation at −1.65 V vs SHE. The reduced consumption of CO_2 in carbonate and bicarbonate formation indicated by the results in Figure 6(e)–(f) and Figure S16 also supports the CO_2 availability in the BL as the consumption of CO_2 in dissociation reactions decreases. However, for the system and parameter space studied here, Figure S14(b) shows that pulsed electrolysis cannot lead to a desired shift from CO_2 consumption to CO_2 production due to dissociation in Reaction (S9) near the electrode, a theory some works stated for CO_2 electrolysis.[43,44] As the forward dissociation rate in Reaction (S9) strongly dominates, transport of CO_2 via HCO_3^- and subsequent local conversion might not be plausible and was also excluded by other groups.[18,45] Therefore, a combination of partial CO_2 replenishment by diffusion from the bulk electrolyte and a reduced CO_2 consumption rate due to a lower pOH in the BL lead to the increase in CO_2 availability at the OHP in Figure 6(d) at short on-pulse duration.

Conclusion

This work presents a transient mathematical model of the BL at a planar plate silver electrode in CO_2 electrolysis. The Frumkin-corrected Tafel equation and the size-modified Poisson-Nernst-Planck model were implemented to resolve mass transport and reactions in the BL. The model was used to elaborate mass transport and reaction phenomena in constant potential and pulsed potential operation. From these results, we deduce trends for optimization of pulsed CO_2 electrolysis based on relevant key performance indicators, i.e. CO current density, Faradaic efficiency, and cathodic energy efficiency. The recent research efforts in pulsed CO_2 electrolysis stem from severe mass transport limitations experienced in constant potential operation. For one, limited CO_2 availability in the immediate electrode environment due to CO_2 solubility and diffusion limitations hamper the CO production rate at elevated potentials in potentiostatic mode. Moreover, CO_2 is steadily consumed in dissociation reactions to HCO_3^- and CO_3^{2-} due to high local alkalinity and sluggish dissociation kinetics. In contrast, the dynamic reorganization of the BL in pulsed operation by alternating replenishment of CO_2 and pH relaxation significantly improves CO_2 availability at the reaction plane. Especially at potentials in the mass transport-limited regime, pulsed electrolysis significantly improves productivity, selectivity, and energy efficiency. These findings suggest that pulsed operation generally benefits electrolysis processes with low reactant solubility, such as electrochemical CO_2 reduction, but the results can also be transferred to N_2 and NO_x reduction. Interestingly, the modulation of the pH by potential pulsing does not lead to a desired local release of CO_2 from HCO_3^- and CO_3^{2-} as often hypothesized but results in a reduction in CO_2 consumption from dissociation.

The results from the symmetric and asymmetric pulses highlight that the pulsed operation mode opens a vast playground to tweak electrolysis performance beyond operating parameters usually modulated in constant potential operation. However, orchestrating the various process parameters is challenging due to the complex interplay of mass transport and reaction phenomena, as shown in this work. Therefore, the model can be useful in holistic mathematical optimization to rapidly deduce optimal pulse operation settings.

Supporting Information

The authors have cited additional references within the Supporting Information.[46–59]

Acknowledgements

This research did not receive any specific grant from funding agencies in the public, commercial, or not-for-profit sectors. The authors acknowledge funding by the Deutsche Forschungsgemeinschaft (DFG, German Research Foundation) under Germany's Excellence Strategy – Exzellenzcluster

2186 'The Fuel Science Center' – ID: 390919832. Wenzel Plischka acknowledges funding through the Horizon Europe project VERGE (no. 101084253). Robert Keller appreciates funding from the Federal Ministry of Education and Research (BMBF) and the Ministry of Culture and Science of the German State of North Rhine-Westphalia (MKW) under the Excellence Strategy of the Federal Government and the Länder. Matthias Wessling acknowledges DFG funding through the Gottfried Wilhelm Leibniz Prize 2019 (WE 4678/12-1). Open Access funding enabled and organized by Projekt DEAL.

Conflict of Interest

The authors declare no conflict of interest.

Data Availability Statement

The model has also been implemented in the non-commercial, open-source modeling framework EnPEn, developed in-house earlier, and is accessible via GitLab (https://git.rwth-aachen.de/avt.cvt/public/ec-enpen). The simulation data is available from the corresponding author upon reasonable request.

Keywords: Electrochemistry · Electric double layer · Modelling · Pulsed electrolysis · Renewable resources

[1] R. I. Masel, Z. Liu, H. Yang, J. J. Kaczur, D. Carrillo, S. Ren, D. Salvatore, C. P. Berlinguette, *Nat. Nanotechnol.* **2021**, *16*, 118.
[2] J. P. Edwards, T. Alerte, C. P. OBrien, C. M. Gabardo, S. Liu, J. Wicks, A. Gaona, J. Abed, Y. C. Xiao, D. Young, et al., *ACS Energy Lett.* **2023**, *8*, 2576.
[3] Y. Xu, J. P. Edwards, S. Liu, R. K. Miao, J. E. Huang, C. M. Gabardo, C. P. OBrien, J. Li, E. H. Sargent, D. Sinton, *ACS Energy Lett.* **2021**, *6*, 809.
[4] C. Kim, J. C. Bui, X. Luo, J. K. Cooper, A. Kusoglu, A. Z. Weber, A. T. Bell, *Nat. Energy* **2021**, *6*, 1026.
[5] A. J. Bard, L. R. Faulkner, J. Leddy, C. G. Zoski, *Electrochemical methods: fundamentals and applications*, volume 2nd ed, Wiley New York **2001**.
[6] R. Casebolt, K. Levine, J. Suntivich, T. Hanrath, *Joule* **2021**, *5*, 1987.
[7] R. Shiratsuchi, G. Nogami, *J. Electrochem. Soc.* **1996**, *143*.
[8] Q. Xu, A. Xu, S. Garg, A. B. Moss, I. Chorkendorff, T. Bligaard, B. Seger, *Angew. Chem. Int. Ed.* **2023**, *62*, e202214383.
[9] X. Lu, C. Zhou, R. S. Delima, E. W. Lees, A. Soni, D. J. Dvorak, S. Ren, T. Ji, A. Bahi, F. Ko, et al., *Nat. Chem.* **2024**, pages 1–9.
[10] P. Sebastián-Pascual, M. Escudero-Escribano, *ACS Energy Lett.* **2019**, *5*, 130.
[11] L. Wang, S. Nitopi, A. B. Wong, J. L. Snider, A. C. Nielander, C. G. Morales-Guio, M. Orazov, D. C. Higgins, C. Hahn, T. F. Jaramillo, *Nat. Catal.* **2019**, *2*, 702.
[12] J. C. Bui, C. Kim, A. Z. Weber, A. T. Bell, *ACS Energy Lett.* **2021**, *6*, 1181.
[13] M. S. Kilic, M. Z. Bazant, A. Ajdari, *Phys. Rev. E* **2007**, *75*, 021503.
[14] D. Bohra, J. H. Chaudhry, T. Burdyny, E. A. Pidko, W. A. Smith, *Energy Environ. Sci.* **2019**, *12*, 3380.
[15] E. N. Butt, J. T. Padding, R. Hartkamp, *Sustain. Energy Fuels* **2023**, *7*, 144.
[16] Z.-X. Luo, Y.-Z. Xing, Y.-C. Ling, A. Kleinhammes, Y. Wu, *Nat. Commun.* **2015**, *6*, 6358.
[17] D. Bohra, J. Chaudhry, T. Burdyny, E. Pidko, W. Smith, *ChemRxiv. Cambridge: Cambridge Open Engage* **2020**.
[18] S. Ringe, C. G. Morales-Guio, L. D. Chen, M. Fields, T. F. Jaramillo, C. Hahn, K. Chan, *Nat. Commun.* **2020**, *11*, 33.
[19] X. Zhu, J. Huang, M. Eikerling, *ACS Catal.* **2021**, *11*, 14521.
[20] T. Yu, H. Tao, J. Li, C. Lian, H. Liu, *Chem. Eng. Sci.* **2023**, page 118759.
[21] H. Wang, A. Thiele, L. Pilon, *J. Phys. Chem. C* **2013**, *117*, 18286.
[22] T. Hatsukade, K. P. Kuhl, E. R. Cave, D. N. Abram, T. F. Jaramillo, *Phys. Chem. Chem. Phys.* **2014**, *16*, 13814.
[23] L.-C. Weng, A. T. Bell, A. Z. Weber, *Phys. Chem. Chem. Phys.* **2018**, *20*, 16973.
[24] K. R. M. Corpus, J. C. Bui, A. M. Limaye, L. M. Pant, K. Manthiram, A. Z. Weber, A. T. Bell, *Joule* **2023**.
[25] C. Kim, L.-C. Weng, A. T. Bell, *ACS Catal.* **2020**, *10*, 12403.
[26] S. Ha, K. Doblhofer, et al., *J. Electroanal. Chem.* **1995**, *380*, 185.
[27] Z. Zhang, L. Melo, R. P. Jansonius, F. Habibzadeh, E. R. Grant, C. P. Berlinguette, *ACS Energy Lett.* **2020**, *5*, 3101.
[28] K. Adamczyk, M. Prémont-Schwarz, D. Pines, E. Pines, E. T. Nibbering, *Science* **2009**, *326*, 1690.
[29] S. Jovanovic, P. Jakes, S. Merz, D. T. Daniel, R.-A. Eichel, J. Granwehr, *Commun. Chem.* **2023**, *6*, 268.
[30] J. Resasco, L. D. Chen, E. Clark, C. Tsai, C. Hahn, T. F. Jaramillo, K. Chan, A. T. Bell, *J. Am. Chem. Soc.* **2017**, *139*, 11277.
[31] C. P. Smith, H. S. White, *Anal. Chem.* **1993**, *65*, 3343.
[32] A. U. Arndt, Ph.D. thesis, FU Berlin (GER) **2022**.
[33] E. R. Cofell, Z. Park, U. O. Nwabara, L. C. Harris, S. S. Bhargava, A. A. Gewirth, P. J. Kenis, *ACS Appl. Energ. Mater.* **2022**, *5*, 12013.
[34] S. Verma, X. Lu, S. Ma, R. I. Masel, P. J. Kenis, *Phys. Chem. Chem. Phys.* **2016**, *18*, 7075.
[35] K. W. Kimura, R. Casebolt, J. Cimada DaSilva, E. Kauffman, J. Kim, T. A. Dunbar, C. J. Pollock, J. Suntivich, T. Hanrath, *ACS Catal.* **2020**, *10*, 8632.
[36] M. R. Singh, J. D. Goodpaster, A. Z. Weber, M. Head-Gordon, A. T. Bell, *Proc. Nat. Acad. Sci.* **2017**, *114*, E8812.
[37] P. Wang, M. Qiao, Q. Shao, Y. Pi, X. Zhu, Y. Li, X. Huang, *Nat. Commun.* **2018**, *9*, 4933.
[38] R. M. Arán-Ais, F. Scholten, S. Kunze, R. Rizo, B. Roldan Cuenya, *Nat. Energy* **2020**, *5*, 317.
[39] H. S. Jeon, J. Timoshenko, C. Rettenmaier, A. Herzog, A. Yoon, S. W. Chee, S. Oener, U. Hejral, F. T. Haase, B. Roldan Cuenya, *J. Am. Chem. Soc.* **2021**, *143*, 7578.
[40] J. Timoshenko, A. Bergmann, C. Rettenmaier, A. Herzog, R. M. Arán-Ais, H. S. Jeon, F. T. Haase, U. Hejral, P. Grosse, S. Kühl, et al., *Nat. Catal.* **2022**, *5*, 259.
[41] Q. Jianping, T. Juntao, S. Jie, W. Cuiwei, Q. Mengqian, H. Zhiqiao, C. Jianmeng, S. Song, *Electrochim. Acta* **2016**, *203*, 99.
[42] D. Frey, K. C. Neyerlin, M. A. Modestino, *React. Chem. Eng.* **2023**, *8*, 323.
[43] M. Dunwell, Q. Lu, J. M. Heyes, J. Rosen, J. G. Chen, Y. Yan, F. Jiao, B. Xu, *J. Am. Chem. Soc.* **2017**, *139*, 3774.
[44] S. Zhu, B. Jiang, W.-B. Cai, M. Shao, *J. Am. Chem. Soc.* **2017**, *139*, 15664.
[45] Y. Hori, S. Suzuki, *J. Electrochem. Soc.* **1983**, *130*, 2387.

[46] D. Bohra, I. Ledezma-Yanez, G. Li, W. de Jong, E. A. Pidko, W. A. Smith, *Angew. Chem. Int. Ed.* **2019**, *131*, 1359.
[47] J. O. Bockris, A. K. Reddy, *Modern Electrochemistry 1: Ionics* **1998**, 2nd edn, vol. 1.
[48] J. B. Hasted, D. M. Ritson, C. H. Collie, *J. Chem. Phys.* **1948**, *16*, 1–21.
[49] S. Trasatti, E. Lust, *Mod. Aspects Electrochem.* **1999**, pages 1–215.
[50] E. F. Johnson, E. Boutin, S. Haussener, *J. Phys. Chem. C* **2023**.
[51] U. Riebesell, V. J. Fabry, L. Hansson, J.-P. Gattuso, *Guide to best practices for ocean acidification research and data reporting*, Office for Official Publications of the European Communities **2011**.
[52] S. Weisenberger, D. A. Schumpe, *AIChE J.* **1996**, *42*, 298.
[53] J. S. Newman, K. E. Thomas-Alyea, *Electrochemical systems*, Electrochemical Society series, Wiley, Hoboken, N. J., 3. ed. edition **2004**.
[54] T. Burdyny, P. J. Graham, Y. Pang, C.-T. Dinh, M. Liu, E. H. Sargent, D. Sinton, *ACS Sustainable Chem. Eng.* **2017**, *5*, 4031.
[55] M. R. Singh, J. D. Goodpaster, A. Z. Weber, M. Head-Gordon, A. T. Bell, *Proc. Nat. Acad. Sci.* **2017**, *114*, E8812.
[56] M. R. Singh, E. L. Clark, A. T. Bell, *Phys. Chem. Chem. Phys.* **2015**, *17*, 18924.
[57] P. W. Atkins, J. De Paula, *Atkins' physical chemistry*, Oxford university press **2014**.
[58] E. Nightingale Jr, *J. Phys. Chem.* **1959**, *63*, 1381.
[59] J. O. Bockris, P. Saluja, *J. Phys. Chem.* **1972**, *76*, 2140.

Manuscript received: April 11, 2024
Accepted manuscript online: June 17, 2024
Version of record online: July 22, 2024